

# Low-loss negative-index metamaterial at telecommunication wavelengths

Gunnar Dolling, Christian Enkrich, and Martin Wegener

Institut für Angewandte Physik, Universität Karlsruhe (TH), Wolfgang-Gaede-Straße 1, D-76131 Karlsruhe, Germany

Costas M. Soukoulis\*

Ames Laboratory and Department of Physics and Astronomy, Iowa State University, Ames, Iowa 50011

Stefan Linden

Institut für Nanotechnologie, Forschungszentrum Karlsruhe in der Helmholtz-Gemeinschaft, Postfach 3640, D-76021 Karlsruhe, Germany

Received February 28, 2006; revised April 3, 2006; accepted April 3, 2006; posted April 5, 2006 (Doc. ID 68552)

We fabricate and characterize a low-loss silver-based negative-index metamaterial based on the design of a recent theoretical proposal. Comparing the measured transmittance and reflectance spectra with theory reveals good agreement. We retrieve a real part of the refractive index of  $\text{Re}(n)=-2$  around  $1.5 \mu\text{m}$  wavelength. The maximum of the ratio of the real to the imaginary part of the refractive index is about three at a spectral position where  $\text{Re}(n)=-1$ . To the best of our knowledge, this is the best figure of merit reported for any negative-index photonic metamaterial to date. © 2006 Optical Society of America

OCIS codes: 160.4760, 260.5740.

In 2005, the first metamaterials exhibiting a negative index of refraction at optical frequencies were reported.<sup>1,2</sup> They all follow the general idea of fabricating an artificial effective material composed of “magnetic atoms,” providing a negative magnetic permeability  $\mu$ , and “electric atoms,” providing a negative electric permittivity  $\epsilon$ . The resulting index of refraction  $n$  is generally complex. Clearly both future physics experiments as well as potential applications (e.g., Pendry’s perfect lens<sup>3</sup>) require that the modulus of the real part  $\text{Re}(n)<0$  is much larger than the imaginary part  $\text{Im}(n)>0$ . In other words, the figure of merit (FOM),

$$\text{FOM} = -\text{Re}(n)/\text{Im}(n), \quad (1)$$

should be as large as possible. For the double-wire design,<sup>2</sup> the maximum value was  $\text{FOM}\approx 0.1$  at  $\text{Re}(n)\approx -0.2$  around  $1.5 \mu\text{m}$  wavelength.<sup>2</sup> A precursor of the structure to be discussed in this Letter gave  $\text{FOM}\approx 0.5$  at  $\text{Re}(n)\approx -1$  around  $1.9 \mu\text{m}$  wavelength.<sup>1</sup> Thus the most prominent next frontier of negative-index metamaterials is to reduce their losses.

In a corresponding recent theoretical study,<sup>4</sup> Zhang *et al.* proposed a novel negative-index metamaterial structure. Depending on the metal damping assumed, values as large as  $\text{FOM}=6$  have been reported.<sup>4</sup> Their design is schematically shown in Fig. 1(a), together with our sample parameters. For the polarization configuration depicted, the structure can be thought of as consisting of double-plate (or double-wire) pairs<sup>5,6</sup> as “magnetic atoms” and long wires as “electric atoms” (just a diluted Drude metal). The key to optimizing the FOM of this structure<sup>4</sup> lies in tuning the combination of wire widths, metal thickness, and spacer thickness. For example, the width of the thin double wires has to be sufficiently large to bring the corresponding effective plasma fre-

quency above the frequency where a negative index is expected [otherwise  $\text{Re}(\epsilon)>0$ ]. This aspect obviously introduces a dependence of the optimization on the metal plasma frequency. On the other hand, this width should be as small as possible to not disturb the performance of the “magnetic atoms.” One major source of line broadening stems from the damping of the constituent metal. Thus low-loss constituent metals are of obvious interest. It is well known that silver has the lowest damping of all metals at optical frequencies. According to measurements<sup>7</sup>

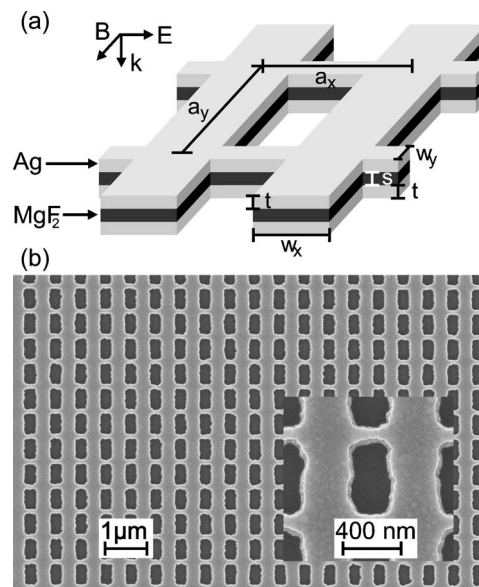


Fig. 1. (a) Scheme of the negative-index metamaterial design and polarization configuration. The sample parameters used in Figs. 2 and 3 are given:  $w_x=316 \text{ nm}$ ,  $w_y=100 \text{ nm}$ ,  $t=45 \text{ nm}$ ,  $s=30 \text{ nm}$ , and lattice constant  $a_x=a_y=600 \text{ nm}$ . (b) Top-view electron micrograph of the silver-based structure. Inset, magnified view.

on thin films at wavelengths of interest here, silver has a damping lower than gold (used in Refs. 1, 2, and 6) by about a factor of four.

Thus we employ silver in this study. Our samples are fabricated on glass substrate, covered with a 5 nm thin film of indium tin oxide, by using standard electron-beam lithography<sup>5,8,9</sup> and electron-beam evaporation of the constituent materials at pressures below  $10^{-6}$  hPa. Each sample has a footprint of  $100\ \mu\text{m} \times 100\ \mu\text{m}$ . In total, we have fabricated about 60 different samples, the results of the best sample are presented below. The electron micrographs of this sample shown in Fig. 1 reveal a high-quality silver film and a width of the thin wires around 100 nm. Furthermore, the large-scale quality of the sample is obviously excellent.

For the optical characterization, we employ polarized broadband white-light normal-incidence transmittance and reflectance spectroscopy. We use a home-built setup that allows for the investigation of small-area samples at a half-opening angle of  $5^\circ$ . For the transmittance measurements, the sample plane is magnified and reimaged onto an intermediate image plane. Adjustable knife edges in this plane ensure that only light that has passed through the sample is actually collected. For both transmittance and reflectance, the collected light is spectrally dispersed with an optical spectrum analyzer (Ando AQ 6315B), giving access to the spectral interval from 900–1700 nm wavelength. Normalization is with respect to the bare glass substrate (for transmittance) and a silver mirror (for reflectance), respectively. Corresponding measured spectra are depicted in Fig. 2(a) for the relevant polarization configuration shown in Fig. 1 (solid curves). The dashed curves in Fig. 2(a) are for the orthogonal incident polarization. Here the light field “sees” an effective metal with large effective plasma frequency, hence low transmittance (high reflectance) over the entire spectral range. These measured spectra are directly compared with numerical calculations [Fig. 2(b)] that are based on the sample design and on the sample parameters given in Fig. 1. We employ a commercial finite-difference time-domain software package (Computer Simulation Technology Microwave Studio) and the Drude model for silver. The plasma frequency is  $\omega_{\text{pl}} = 1.37 \times 10^{16}\ \text{s}^{-1}$ ,<sup>7</sup> while the collision frequency is  $\omega_{\text{col}} = 8.5 \times 10^{13}\ \text{s}^{-1}$ . The latter has been used as a free parameter. The resulting choice is somewhat larger than that of the literature<sup>7</sup> and effectively subsumes other broadening channels, such as inhomogeneous broadening due to fabrication tolerances [see Fig. 1(b)]. The refractive index of the glass substrate is  $n = 1.48$ , and that of the  $\text{MgF}_2$  dielectric spacer layer is  $n = 1.38$ . It is apparent that the overall agreement between experiment and theory in Fig. 2 is extremely good. This is true for both transmittance and reflectance, for the relevant incident polarization, and for the orthogonal incident polarization.

This gives us sufficient confidence into the theory to retrieve<sup>10,11</sup> the effective metamaterial parameters from the theory for the relevant linear polarization. The basic idea underlying the retrieval is simple: for

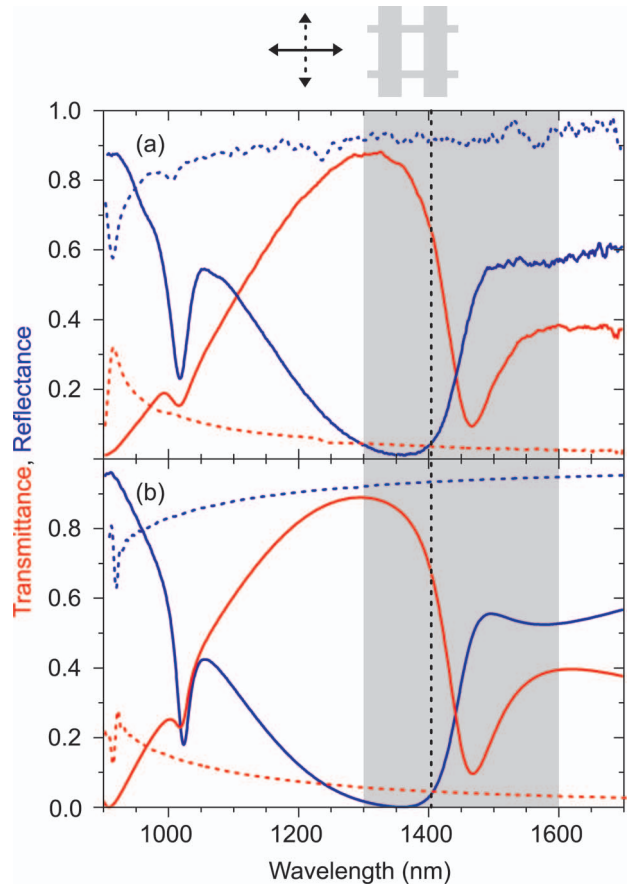


Fig. 2. (a) Measured normal-incidence transmittance (red) and reflectance (blue) spectra for the incident polarization configuration (solid curves) depicted in Fig. 1(a); dashed curve, orthogonal linear polarization. (b) Corresponding calculated spectra. Gray area, spectral region shown in Fig. 3; dashed vertical line, position of  $\text{Re}(n) = -1$ , where the FOM is  $\sim 3$ .

known complex permittivity  $\epsilon$  and permeability  $\mu$  (hence known as complex refractive index  $n$  and impedance  $Z$ ), it is straightforward to compute the normal-incidence complex field transmittance and reflectance for a slab of (meta)material of thickness  $d$  at any given frequency (here  $d = 2t + s = 120\ \text{nm}$ ). The inversion of this problem is generally not unique, and physical conditions have to be imposed. For example,<sup>10,11</sup>  $\epsilon(\omega)$  and  $\mu(\omega)$  must not reveal discontinuous spectral jumps and, for a passive medium,  $\text{Im}(n) \geq 0$  must hold. However, as electric and magnetic dipoles are not independent in metamaterials, this condition can be fulfilled while, e.g.,  $\text{Im}(\epsilon) < 0$ . This unusual aspect has been discussed in the literature several times.<sup>10,11</sup> If the metamaterial slab is additionally located on a substrate, the complex field reflectance for a wave impinging from one side is generally not identical to that from the opposite side. To avoid problems related to this ambiguity, we embed the metamaterial structure in an effective homogeneous medium (also see Ref. 4) with refractive index 1.05. Using a vacuum would slightly blue shift all resonances, hindering a direct comparison with Fig. 2. Figure 3 shows the retrieved complex parameters. For the spectral interval shown, the corresponding

calculated intensity transmittance and reflectance spectra (not shown) are closely similar to those calculated for the half-space geometry (Fig. 2). Notably, we obtain a refractive index  $\text{Re}(n) \approx -2$  around  $1.45 \mu\text{m}$  wavelength in Fig. 3(c). As expected,  $\epsilon$  in Fig. 3(a) closely resembles the permittivity of a diluted Drude metal, whereas  $\mu$  [Fig. 3(b)] exhibits a magnetic resonance behavior that has been described previously.<sup>2,5,6</sup> The interaction of the electric and the magnetic response leads to a negative imaginary part of  $\epsilon$  close to the magnetic resonance (see discussion above). Most important, Fig. 3(d) exhibits the FOM. It reaches a maximum of  $\text{FOM} \approx 3$  at a spectral position where  $\text{Re}(n) \approx -1$ , as, e.g., requested for Pendry's perfect lens.

In conclusion, we have realized a negative-index metamaterial at telecommunication wavelengths. This metamaterial is based on silver rather than gold as the constituent metal. The experimental results agree very well with theory. We achieve  $\text{FOM} \approx 3$ . To the best of our knowledge, this is the largest value reported for any photonic metamaterials to date.

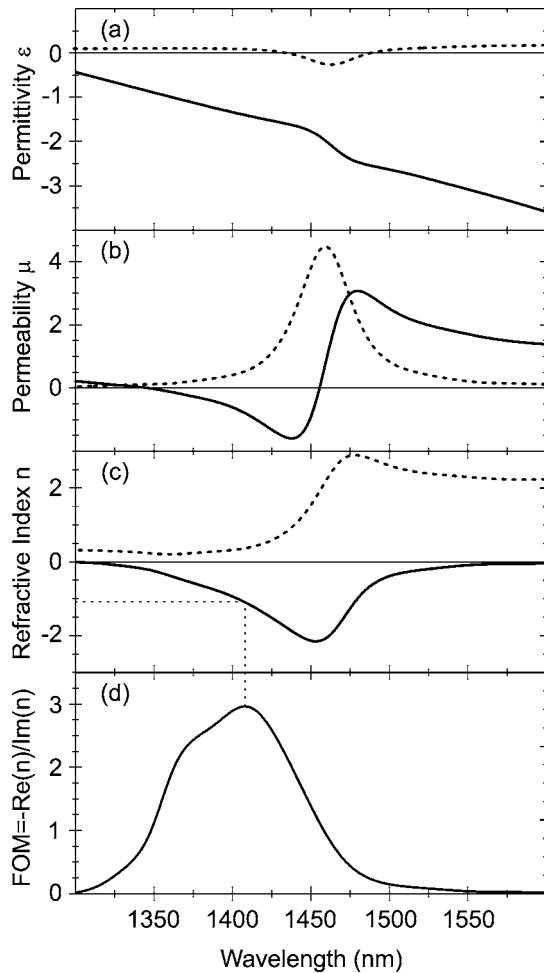


Fig. 3. (a) Retrieved permittivity  $\epsilon$ , (b) retrieved magnetic permeability  $\mu$ , and (c) refractive index  $n$ . Solid curves, real parts; dashed curves, imaginary parts. (d) FOM.

We acknowledge support by the Deutsche Forschungsgemeinschaft (DFG) and the State of Baden-Württemberg through the DFG-Center for Functional Nanostructures (CFN) within subproject A 1.5. M. Wegner's research is further supported by project DFG-We 1497/9-1 and S. Linden's research is supported by a Helmholtz-Hochschul-Nachwuchsgruppe (VH-NG-232) C. M. Soukoulis's research is further supported by the Alexander von Humboldt Distinguished Senior Scientist Award (2002) by Ames Laboratory (contract W-7405-Eng-82) and European project DALHM, Metamorphose, and Phoremest, and Defense Advanced Research Projects Agency (HR0011-05-C-0068). G. Dolling's e-mail address is [gunnar.dolling@physik.uni-karlsruhe.de](mailto:gunnar.dolling@physik.uni-karlsruhe.de).

*Note added in proof:* After submission of this manuscript, we performed additional femtosecond-pulse-propagation experiments on the silver-based metamaterial sample. By analyzing the fringes and the envelopes of the interferograms with and without the sample in one arm of a Michelson interferometer, we determined both phase and group time delay for many different wavelengths. These experimental results are also in excellent agreement with the theory outlined in this Letter, further supporting the claims of the Letter.

\*C. M. Soukoulis is also at the Institute of Electronic Structure and Laser at FORTH, and Department of Materials Science and Technology, University of Crete, Heraklion, Crete, Greece.

## References

1. S. Zhang, W. Fan, N. C. Panoiu, K. J. Malloy, R. M. Osgood, and S. R. J. Brueck, *Phys. Rev. Lett.* **95**, 137404 (2005).
2. V. M. Shalaev, W. Cai, U. K. Chettiar, H. Yuan, A. K. Sarychev, V. P. Drachev, and A. V. Kildishev, *Opt. Lett.* **30**, 3356 (2005).
3. J. B. Pendry, *Phys. Rev. Lett.* **85**, 3966 (2000).
4. S. Zhang, W. Fan, K. J. Malloy, S. R. J. Brueck, N. C. Panoiu, and R. M. Osgood, *Opt. Express* **13**, 4922 (2005).
5. G. Dolling, C. Enkrich, M. Wegener, J. Zhou, C. M. Soukoulis, and S. Linden, *Opt. Lett.* **30**, 3198 (2005).
6. A. N. Grigorenko, A. K. Geim, H. F. Gleeson, Y. Zhang, A. A. Firsov, I. Y. Khrushchev, and J. Petrovic, *Nature* **438**, 335 (2005).
7. P. B. Johnson and R. W. Christy, *Phys. Rev. B* **6**, 4370 (1972).
8. S. Linden, C. Enkrich, M. Wegener, J. Zhou, T. Koschny, and C. M. Soukoulis, *Science* **306**, 1351 (2004).
9. C. Enkrich, M. Wegener, S. Linden, S. Burger, L. Zschiedrich, F. Schmidt, J. Zhou, T. Koschny, and C. M. Soukoulis, *Phys. Rev. Lett.* **95**, 203901 (2005).
10. D. R. Smith, D. C. Vier, Th. Koschny, and C. M. Soukoulis, *Phys. Rev. B* **71**, 036617 (2005).
11. Th. Koschny, P. Markos, E. N. Economou, D. R. Smith, D. C. Vier, and C. M. Soukoulis, *Phys. Rev. B* **71**, 245105 (2005).